PAPER

CrossMark
click for updates

Assessment of the toxicity and inflammatory effects of different-sized zinc oxide nanoparticles in 2D and 3D cell cultures

Zhipan Wu,†[a] Rongfa Guan,†*[a] Miao Tao,†[a] Fei Lyu,[b] Guozhou Cao,[c] Mingqi Liu[a] and Jianguo Gao[d]

Two-dimensional (2D) monolayer cell cultures are the most common *in vitro* models for mechanistic studies on the toxicity of engineered nanoparticles (NPs). However, 2D cell cultures may not accurately model the functions of three-dimensional (3D) tissues that have extensive cell–cell and cell–matrix interactions, and thus may lead to wrong experimental results. Hence, to obtain more adequate and detailed information about ZnO NP–tissue interactions, we here assess the toxicity and inflammatory effects of different-sized ZnO NPs at various concentrations on Caco-2 cells which are three-dimensionally cultured in agarose gels, measuring ROS expression, pro-inflammatory cytokines, cell proliferation and death. The results showed that the significant effects of cell dimensionality to cellular responses such as inflammatory response, cytotoxicity and different modes of cell death in response to ZnO NPs treatment. Moreover, ZnO NPs induced the toxicity of 2D and 3D cells in different size-dependent manners. This study revealed that the nanotoxicity conclusions obtained from the 2D cell model might overestimate the toxic effects of ZnO NPs. There is a more realistic mechanism study of nanoparticle-induced toxicity in the 3D cell model, which acts as an intermediate stage bridging *in vitro* 2D and *in vivo* models.

1. Introduction

Zinc oxide nanoparticles (ZnO NPs) have been used in the field of catalysis, sunscreen cosmetics, paint materials, and food packaging materials because of their unique optical, electrical, and thermal performance.[1,2] Nanoparticles have a strong influence on the way they interact with biological components,[3] and it raises a real concern about the risk to human health from the inevitable exposure to NPs.[4] The inconsistencies among culture dish assessments, animal trials, and consumers' perceived experience after exposure to these NPs constitute burden for defining the biological effects and underlying toxic mechanisms of NPs.[5] ZnO NPs have good antimicrobial activity that can be utilized as agents to prevent harmful microorganism growth in food.[6]

However, the use of ZnO NPs as food additive is limited by the perceived high toxicity of ZnO NPs in many earlier toxicity studies.[6–9] Two-dimensional (2D) monolayer cell model have a very low anatomical and physiological relevance, while they remain the predominant *in vitro* model for numerous nanotoxicity studies.[10,11] However, cells lose their original tissue organization, polarity, and protein–protein interactions in the case of 2D cell culture on a flat substrate, which in turn significantly limits their ability to recapitulate the appropriate level of *in vivo* cellular responses.[12] Due to the absence of cell–cell and cell–matrix interactions, tests based on *in vitro* 2D cell culture model do not accurately predict *in vivo* toxicity and other biological effects despite of providing valuable and important information.[13,14] Therefore, a more tissue-like, physiologically relevant model which can mimic the interactions between biological systems and NMs is most needed.

Virtually all cells reside in a three-dimensional (3D) milieu of the body and sophisticated interactions with 3D organized extracellular matrix (ECM) proteins and neighboring cells is critical for the phenotype and function of individual cells.[15,16] However, organ culture (*ex vivo*) to obtain and scale up the specimen for multiparametric studies is generally more difficult.[17] 3D cell culture model such as microtissue spheroid which emulates the complex *in vivo* cellular organization is easier to be established in a laboratory than organ culture. Previous study reported that the enhanced specific protein secreting function

[a]*Zhejiang Provincial Key Laboratory of Biometrology and Inspection & Quarantine, College of Life Sciences, China Jiliang University, Xueyuan Road 258, Hangzhou 310018, China. E-mail: wuzhipanjl@126.com; taomfood@126.com; mqliu524@163.com; Rongfaguan@163.com; Fax: +86-571-8691449*

[b]*Ocean College, Zhejiang University of Technology, Hangzhou 310014, China. E-mail: lvfei_zju@163.com*

[c]*Ningbo Entry–Exit Inspection and Quarantine Technology Center, Ningbo 315000, China. E-mail: caogz@nbciq.gov.cn*

[d]*Inspection and Quarantine Center of Shandong Exit & Entry Inspection and Quarantine Bureau, Qingdao 266002, Shandong province, China. E-mail: china.gjg@163.com*

† Equal contributors.

of granular epithelial cells could only be observed when they formed a 3D organized acinus structure.[18,19] Additionally, an important reason of expanding cell toxicity assays from 2D to 3D cultures is a large discrepancy in toxicity results between *in vitro* 2D cell culture and *in vivo* animal models.[20] For example, 2D cell models were previously reported to showed high cytotoxic effects on toxicity testing of magnetic NPs,[21] carbon nanotubes,[22] and fullerenes,[23] while no adverse effects were observed in animal models.[24–26] Thus, 3D cell culture model is a promising and valuable approach to explore the complex interactions between cells and NPs.

3D cell culture models were previously reported to bridge the gap between 2D cell culture and *in vivo* models.[27] For instance, these cell-to-cell and cell-to-matrix interactions could be better mimicked in the case of 3D cell model.[28] Cellular polarity could be induce in cellular microenvironment of a 3D cell model, and then in favor of tissue organization and the directed secretion of products.[29] Obviously, these examples indicated that 3D cell culture models could be as a more valid and realistic for nanotoxicity studies. One study has reported the *in vitro* ZnO NPs toxicity testing using 2D cell culture,[30] so it will be very important to use 3D cell model for the toxicity assessment of ZnO NPs and compare the results with 2D cell culture.

In this study, the assessment of toxicity and inflammatory effects of different sized ZnO NPs at various concentrations (0, 10, 25, 50, 75, or 100 µg mL^{-1}) on Caco-2 cells, three-dimensionally cultured in agarose gels, was evaluated by measuring ROS expression, pro-inflammatory cytokines, cell proliferation and death.

2. Materials and methods

2.1. Characterization of ZnO NPs

A stock suspension of ZnO NPs (final concentration, 400 µg mL^{-1}; Shanghai Jingchun Biochemical Technology Company, Shanghai, China) was prepared in phosphate-buffered saline (PBS, Sigma, USA). Prior to each treatment, the suspension was ultrasonicated before exposure (amplitude, 100%; pulse, 5 s/10 s; 2 min) and diluted to prepare the desired ZnO NP concentrations (10, 25, 50, 75, and 100 µg mL^{-1}) in serum-free medium without L-glutamine and antibiotics. Particle morphology, size, and agglomeration states were characterized *via* transmission electron microscopy (TEM, JEOL JEM-2100, JEOL Ltd., Tokyo, Japan). Samples for TEM analysis were prepared through anhydrous ethanol ultrasonic dispersion onto standard holey carbon-coated copper grids, which were then air-dried at room temperature. The intensity and size of the particles were analyzed using a Malvern Zetasizer (Worcestershire, UK).

2.2. Cell culture

Cell preparation. Caco-2 cells were derived from a human epithelial colorectal adenocarcinoma (The Type Culture Collection of the Chinese Academy of Sciences, Shanghai, China). The cells were cultured in Dulbecco's modified Eagle's medium (DMEM, Gibco BRL, Gaitherburg, MD, USA) supplemented with 10% fetal bovine serum (FBS, Hyclone Laboratories, Inc., USA)

and 1% antibiotics (Sigma, USA), maintained at 37 °C in an atmosphere of 95% air and 5% CO$_2$ in 75 cm^2 flasks, and then sub-cultured once every 3 days at 80% confluence.

2D cell culture. Caco-2 cells were isolated using 0.05% Trypsin–EDTA (Sigma, USA) and centrifuged at 2000 rpm for 2 min. Isolated cells were seeded at 24-well and 96-well plate according to the experimental design. The cells were then cultured using DMEM supplemented with 10% FBS, 1% antibiotics (100 IU mL^{-1} penicillin, 100 µg mL^{-1} streptomycin), maintained at 37 °C in an atmosphere of 95% air with 5% CO$_2$. The medium was replaced every 3–4 days. All of the experiments were performed on logarithmically growing cells. The prepared cells were exposed to various ZnO NP concentrations (0, 10, 25, 50, 75, or 100 µg mL^{-1}).

3D cell culture. Caco-2 cells were isolated as previously described. The cells of seeding density 2×10^5 cells per mL, were then immobilized in a 1% agarose gel casted by using 3D Petri dish (Sigma, USA), which contained 96 small wells. A portion of the cell suspension containing 1×10^5 cells/500 µL was added to an equal volume of sterilized, and molten (37 °C), 2% (w/v) agarose in PBS solution (Sigma, USA).[31,32] A 500 µL aliquot of the mixture was then loaded into a 24-well plate fitted into the 3D Petri dish and kept at room temperature for 30 min to allow the gel to solidify. The cells were then cultured using DMEM supplemented with 10% FBS, and 1% antibiotics maintained at 37 °C in an atmosphere of 95% air with 5% CO$_2$. The medium was replaced every 3–4 days. All of the experiments were performed on logarithmically growing cells. The prepared cells were exposed to various ZnO NP concentrations (0, 10, 25, 50, 75, or 100 µg mL^{-1}). Agarose is acts as a scaffold for cell culture, so that 3D cell culture has possibility. Cell matrix provides cell culture environment a third dimension. There are several main types of cell matrix, including hydrogel scaffold from natural materials, such as extracellular matrix collagen; second type of cell matrix is synthetic hydrogel, including bionic peptide, sometimes they can strengthen the combination of integrin. Other types of artificial scaffold are plastic from tissue culture, and even biodegradable plastics.

2.3. Characterization of Caco-2 cells

Caco-2 cells were cultured on 2D and 3D microstructured substrates. Microstructures were generated by XDS-100 invert microscope (Shanghai Cai Kang Optical Instrument Company, China). Using inverted microscope to observe the morphology of Caco-2 cells under 2D and 3D circumstances.

2.4. ROS assay

Intracellular reactive oxidative stress (ROS) expression level was detected and measured, using the redox sensitive CellROX orange reagent that fluoresces brightly when exposed to ROS. Caco-2 cells were seeded in 96-well plate format (2D) or agarose gel cultured format (3D) as previously described. The cells were treated with three sizes of ZnO NPs at various concentrations (0, 10, 25, 50, 75, or 100 µg mL^{-1}) for 6 and 12 h. At the end of the treated time, CellROX orange reagent (Reactive Oxygen Species Assay Kit, Beyotime Company, Shanghai, China) were added

directly to every well and then, the samples were incubated at 37 °C and protected from light for 30 min. Thereafter, the staining solution was removed and the cells was washed three times using ice-cold PBS. The samples were observed under a fluorescence microscope (Nikon Eclipse Ti, Nikon, Shinjuku, Tokyo, Japan) and the data were expressed as ROS-positive cells.

2.5. Measurement of pro-inflammatory cytokines

Interleukin-8 (IL-8) and Interleukin-1β (IL-1β) are pro-inflammatory cytokines correlated with inflammatory potential of particles.[33] 2D and 3D cells were treated with 24 nm, 56 nm and 87 nm ZnO NPs (the average particle size) at various concentrations (0, 10, 25, 50, 75, or 100 μg mL^{-1}) for 12 and 24 h. At the end of the treated time, 2D and 3D cells were trypsinized by trypsin–EDTA and the trypsinized cells were neutralized with completed DMEM. The cells mixture was centrifuged to remove supernatant, then washed and centrifuged twice using 1× PBS to remove all traces of the medium. The cell pellet was sonicated at 300 W for 10 s (3 cycles) to obtain lysates, which were then centrifuged at 1000 rpm for 10 min to obtain the supernatant. We measured IL-8 protein levels and IL-1β in the supernatant of 2D and 3D cells according to the instruction manual (R&D Systems).

2.6. Cell proliferation

DNA quantification was performed to assess cell proliferation using the Quant-iT PicoGreen dsDNA reagent and kit (Molecular Proves, Eugene, OR, USA). DNA quantification was measured *via* fluorescent expression of PicoGreen dye binding to cellular nucleic acids assay. Caco-2 cells were seeded in 96-well plate format (2D) or agarose gel cultured format (3D) as previously described. The cells were treated with 24 nm ZnO NPs (the average particle size) at various concentrations (0, 10, 25, 50, 75, or 100 μg mL^{-1}) for 12 and 24 h. Then, in the 3D agarose gel cultured model, the cells encapsulated in agarose gel were directly digested in papain buffer without any prior extraction. The cell samples were placed in 1.5 mL sterile Eppendorf tubes at 37 °C for 5 min with 1 mL of papain digestion buffer (100 mM Na$_2$HPO$_4$, 5 mM L-cysteine, 5 mM EDTA, pH 7.5) containing 125 μg mL^{-1} papain type III. Following digestion, the samples were heated to 60 °C for 10 min to melt the agarose. In 2D cell model, the cells were digested as in the previously described 3D cultured model. Then the samples were centrifuged at 5000*g* for 2 min at room temperature. Exactly 100 μL of the supernatant and 100 μL of PicoGreen fluorescence reagent (1 : 200 in Tris–EDTA buffer, Invitrogen Co., NY, USA) were added to each well of 96-well plate, and the mixture was mixed thoroughly. Fluorescence was measured in a multi-detection reader (Synergy HT BioTek, Winooski, VT, USA). DNA standards were prepared using the same procedure and sample values were calculated using the known DNA standards.

2.7. Modes of cell death

An AnnexinV-FITC/Propidium Iodide (PI) detection kit was used to quantify different modes of cell death.[34] 2D and 3D cells were treated with 24 nm, 56 nm and 87 nm ZnO NPs (the average

particle size) at various concentrations (0, 10, 25, 50, 75, or 100 μg mL^{-1}) for 24 h. After 24 h of incubation, all treated 2D and 3D cells were trypsinized by trypsin–EDTA at 37 °C. The trypsinized cells were then neutralized with completed DMEM, collected *via* centrifugation, washed with 1× PBS and subsequently resuspended in 100 μL of binding buffer. Exactly 5 μL of AnnexinV-FITC and 10 μL of PI solution were added into the cell suspension. After 15 min of incubation at room temperature in the dark according to the manufacturer's instructions, cell apoptosis was immediately analyzed by using a flow cytometer (Partech GmbH, Germany).

3. Results

3.1. Characterization of ZnO NPs

TEM was conducted to investigate the morphology of the ZnO NPs, and size distribution was assessed using a Malvern instrument. Fig. 1 shows representative TEM images of the ZnO NPs. The ZnO NPs showed the following average particle diameters: (a) 24.49 ± 2.54 nm, (b) 56.11 ± 8.56 nm, and (c) 87.26 ± 13.47 nm. Fig. 1d–f showed nanoparticles of different sizes. Thus, 24, 56, and 87 nm ZnO NPs were used in the following test system.

3.2. Characterization of Caco-2 cells

As Fig. 2a and b show, Caco-2 cells in 2D culture plate, form a cell model of monolayer, firm, adherent, and present fusiform or polygonal; Caco-2 cells in 3D culture, form larger and spherical cell masses. After 10 μg mL^{-1} ZnO NPs (24 nm average particle size) affecting 2D and 3D cells, compared with the control groups (Fig. 2a and b), 2D cellular morphology has good adherence, no obvious change, but refractive index becomes worse, gap bigger, some cells become smaller and more round; the form of 3D cells almost no change (Fig. 2c and d). As shown in Fig. 2e and f, when the virus concentration increased to 75 μg mL^{-1}, in the 2D model, can discover black and conglobatus ZnO NPs (24 nm average particle size), necrosis in morphology, different degree of crushing, lower adherence, "dirty", populations decrease; 3D cells still does not have obvious changes in morphology, but the cell clusters are smaller.

3.3. ROS expression

ROS-positive cells are defined as cells with measured ROS expression levels higher than a pre-determined fluorescence threshold value. As shown in Fig. 3, significant increased ROS levels was observed in 2D format, but not for Caco-2 cells in 3D culture after both 6 h and 12 h of ZnO NPs exposure. Caco-2 cells cultured in 3D possessed a higher basal level of ROS expression as compared to the cells in 2D at low concentrations (around 10 μg mL^{-1} ZnO NPs), even the untreated 3D control. Surprisingly, the difference in endogenous ROS levels of 2D cells is much lower (2.9%, 3.2% and 3.3%, control groups at 6 h) and not as significant ($p > 0.25$) as the one observed in 3D cell model (Fig. 3a, c and e). 24 nm ZnO NPs (the average particle size) treatment increased the highest percentage of oxidative stressed cells compared to 56 nm and 87 nm ZnO NPs (the
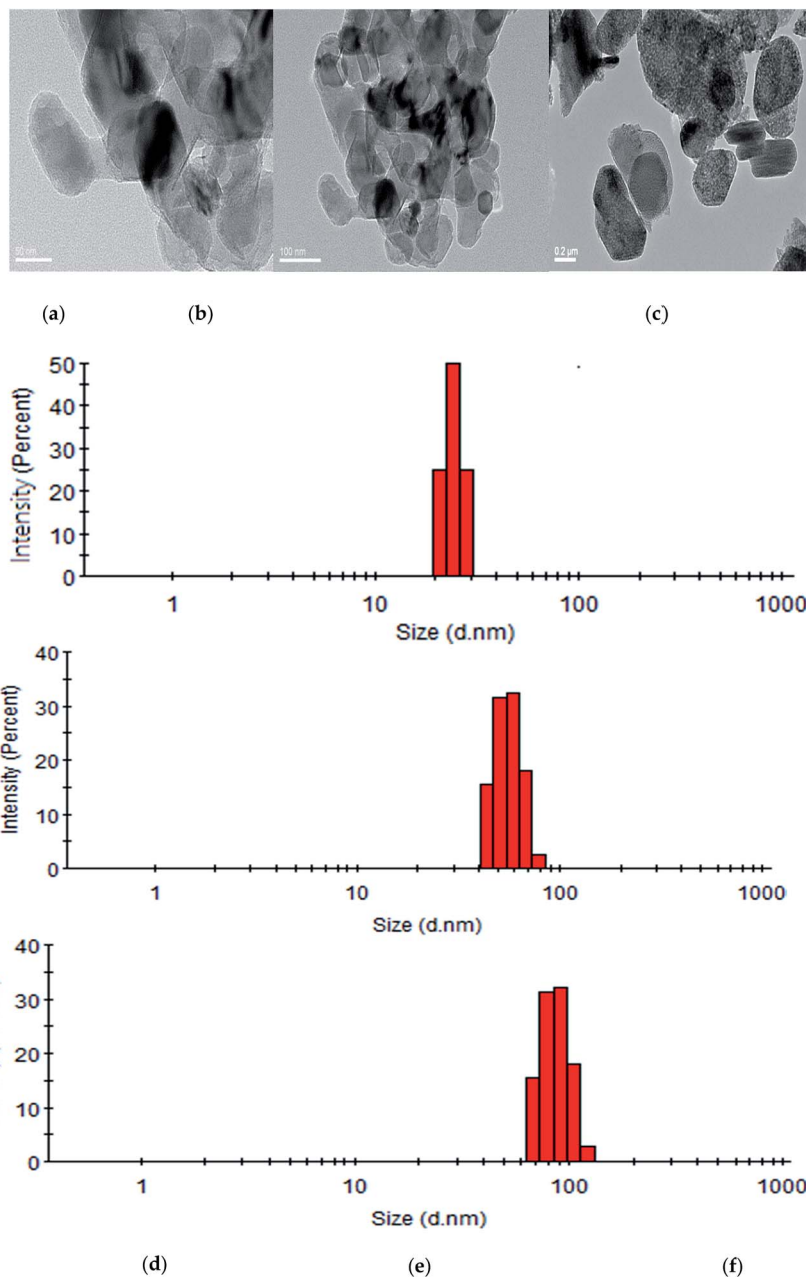
Fig. 1 Microscopy characterizations of ZnO NPs. TEM images of an average: (a) 24 nm ZnO NPs (the average particle size), (b) 56 nm ZnO NPs (the average particle size), and (c) 87 nm ZnO NPs (the average particle size). Ranges: (d) 20–30 nm for a nanoparticle, (e) 40–70 nm for a nanoparticle, and (f) 70–100 nm for a nanoparticle. TEM scale bars: (a) 50 nm, (b) 100 nm, and (c) 0.2 μm.

average particle size) in 2D cell model after 6 h and 12 h exposure, and in 3D culture after 12 h exposure (Fig. 3b and f).

3.4. Pro-inflammatory cytokines

Fig. 4 showed that ZnO NPs trigger differential expression of IL-8 and IL-1β between in 2D and 3D cell model. In this study, the total protein amount averagely was 74 μg/10^5 cells. After 12 h of high concentrations of ZnO NPs (above 50 μg mL^{-1} ZnO NPs) treatment, the levels of IL-8 and IL-1β protein in the supernatant were significantly increased in 2D and 3D cell model except 2D cells for IL-8. We observed that More than a 5-fold and 9-fold

increase of IL-8 and IL-1β protein, respectively, were induced by 100 μg mL^{-1} of 24 nm ZnO NPs (the average particle size) in 3D cell model, but less in 2D cell culture after 12 h of exposure (Fig. 4a and e). 24 nm ZnO NPs (the average particle size) treatment increased higher levels of IL-8 and IL-1β than 87 nm ZnO NPs in 3D cell model, but no similar result was observed in 2D cell model after 12 h exposure (Fig. 4a, c, e and h). ZnO NMs induced severe inflammatory responses to in 3D cell format after 12 h of exposure, while it did not cause a significant increase of ROS-positive cells at the same time point (Fig. 3b, d and f). These results implied that ZnO NPs could induce an
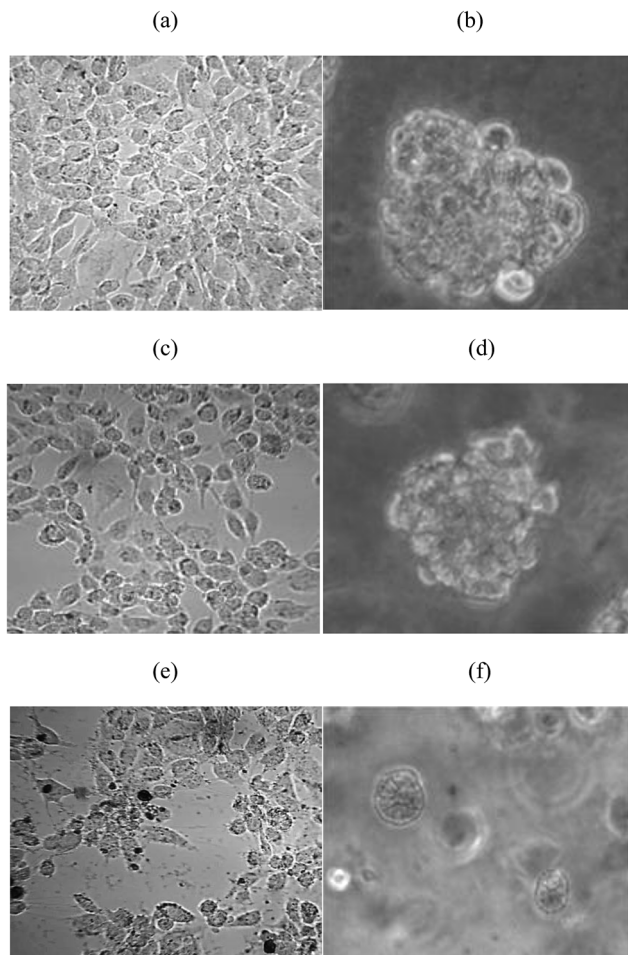
Fig. 2 Microscopy characterizations of Caco-2 cells under 2D and 3D circumstances. (a) Normal Caco-2 cells at 2D cell culture, (b) normal Caco-2 cells at 3D cell culture, (c) after 10 µg mL^{-1} ZnO NPs (24 nm average particle size) affecting 12 h, Caco-2 cells at 2D cell culture, (d) after 10 µg mL^{-1} ZnO NPs (24 nm average particle size) affecting 12 h, Caco-2 cells at 3D cell culture, (e) after 75 µg mL^{-1} ZnO NPs (24 nm average particle size) affecting 12 h, Caco-2 cells at 2D cell culture, (f) after 75 µg mL^{-1} ZnO NPs (24 nm average particle size) affecting 12 h, Caco-2 cells at 3D cell culture.
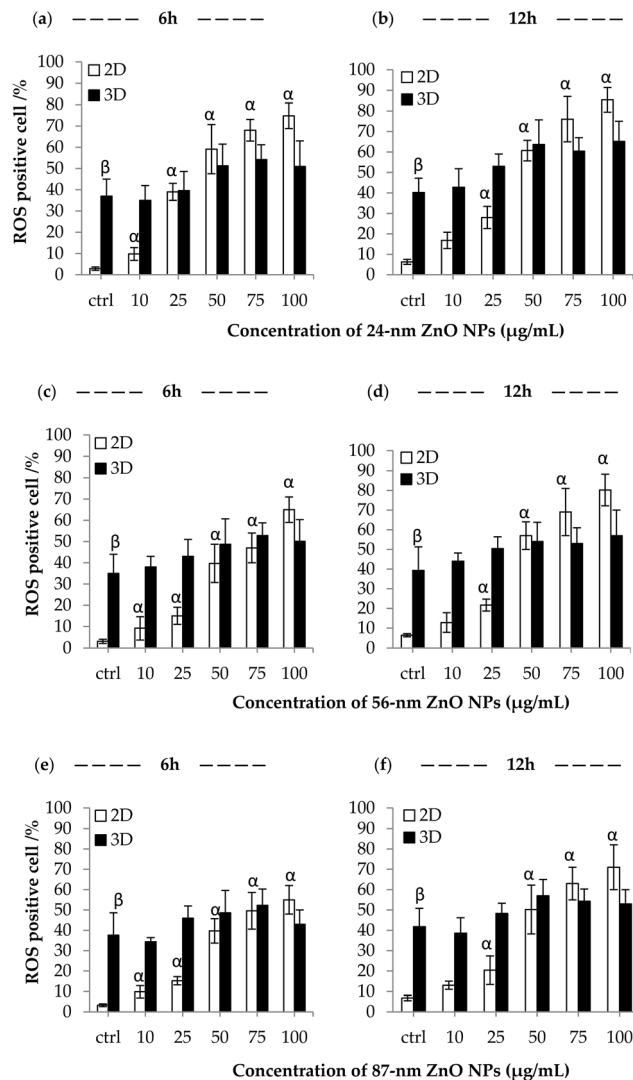

Fig. 3 Intracellular ROS levels to ZnO NPs exposure in 2D and 3D cell model. ROS-positive cells of 2D and 3D cells were observed with various ZnO NP concentrations after exposure to (a) 24 nm ZnO NPs (the average particle size) at 6 h, (b) 24 nm ZnO NPs (the average particle size) at 12 h, (c) 56 nm ZnO NPs (the average particle size) at 6 h, (d) 56 nm ZnO NPs (the average particle size) at 12 h, (e) 87 nm ZnO NPs (the average particle size) at 6 h, (f) 87 nm ZnO NPs (the average particle size) at 12 h. Data represent mean ± SE, n = 3. $p <$ 0.05, β significantly different between the two control groups, α significantly different from control group (ctrl).

inflammatory response which bypassed the increase of ROS levels in 3D cell culture.

When ZnO NPs treatment was extended to 24 h, the levels of IL-8 and IL-1β were further increased in 2D cell model, whilst decrease of the two protein was observed in 3D cell model and the levels of IL-8 were even lower than the basal level of the control groups by 24 nm ZnO NP (the average particle size) at 100 µg mL^{-1} (Fig. 4b). 24 nm ZnO NPs (the average particle size) exposure increased higher levels of IL-8 and IL-1β than 87 nm ZnO NPs (the average particle size) in 2D cell model, however, less levels of IL-8 than 87 nm ZnO NPs (the average particle size) in 3D culture at 24 h (Fig. 4b, d, f and g).

3.5. Cell proliferation

Fig. 5 showed the changes in DNA quantity (cell proliferation) in the 2D and 3D cell model, with 24 nm ZnO NPs (the average particle size) at various concentrations (0, 10, 25, 50, 75, or 100 µg mL^{-1}) after 12 and 24 h of exposure. In 2D cell model, the amount of DNA was decreased ($p < 0.05$) at various concentrations of ZnO NPs in a dose-dependent manner, especially the amount significantly decreased ($p < 0.05$) onset at 75 µg mL^{-1} of ZnO NPs at 12 h and 50 µg mL^{-1} of ZnO NPs at 24 h as compared to the 0 µg mL^{-1} ZnO NPs control. As shown in Fig. 5a, there were no significant differences in the amount of DNA ($p > 0.05$) among various concentrations of ZnO NPs after 12 h of exposure in 3D cell model. The DNA amounts in the 3D cells incubated with low concentrations of ZnO NPs (below 50 µg mL^{-1}) were similar to the control, but incubated with high
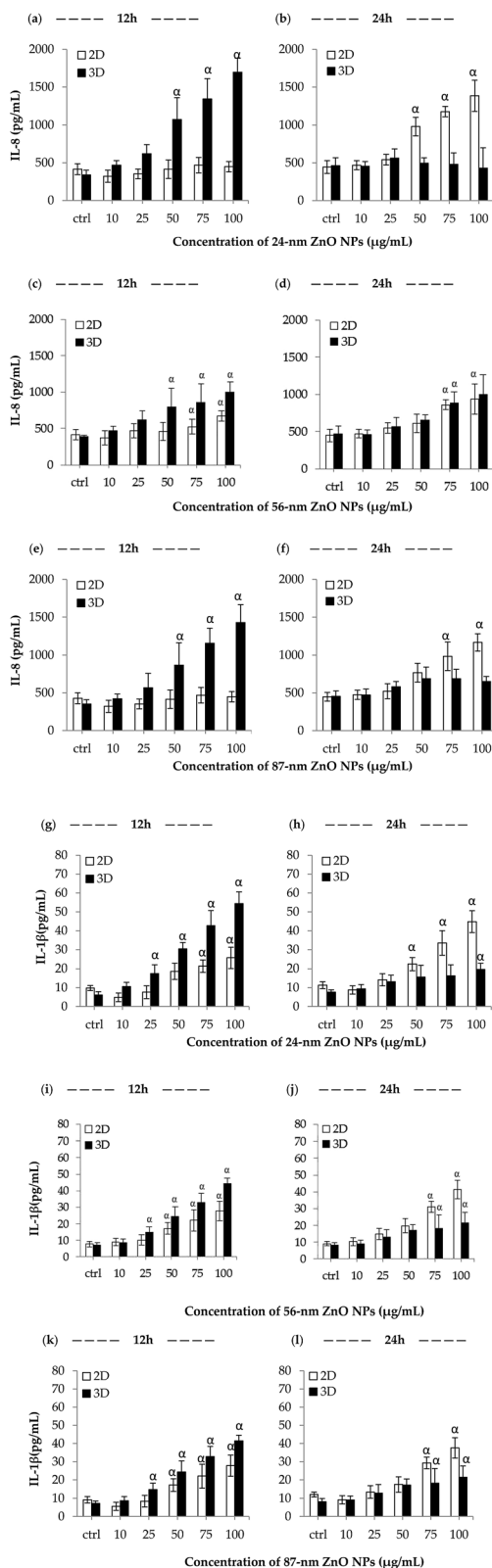
Fig. 4 IL-8 and IL-1β expression of 2D and 3D cells after exposure to ZnO NPs. Levels of IL-8 of 2D and 3D cells with various ZnO NP concentrations after exposure to 24 nm ZnO NPs (the average particle size) at (a) 12 h, or (b) 24 h, 56 nm ZnO NPs (the average particle size) at (c) 12 h, or (d) 24 h, and 87 nm ZnO NPs (the average particle size) at (e) 12 h, or (f) 24 h. Levels of IL-1β of 2D and 3D cells after exposure to 24 nm ZnO NPs (the average particle size) at (g) 12 h, or (h) 24 h, 56 nm

concentrations of ZnO NPs (75 and 100 μg mL^{-1}) decreased as compared to the control after 12 h of exposure (Fig. 5a). Upon 24 h of ZnO NPs treatment, the amount of DNA was significantly decreased at the highest concentration of ZnO NPs (100 μg mL^{-1}) in 3D cell model, but at 50 μg mL^{-1} of ZnO NPs in 2D cell model (Fig. 5b).

3.6. Modes of cell death

As shown in Fig. 6, Annexin V-FITC/PI assay captured the different cell death profile in 2D and 3D cell model, and implied that Caco-2 cells responded to ZnO NPs toxicity in a dose-dependent manner, regardless of the cell model used after 24 h of treatment. However, higher cell death was observed in 2D cell model as compare to 3D cell model. 24 nm ZnO NPs (the average particle size) exposure increased higher levels of cyto-toxicity than 87 nm ZnO NPs (the average particle size) in 2D cell model, but both were similar levels in 3D culture. Almost no early apoptotic cells were observed in the 2D model onset at 75 μg mL^{-1} of 24 nm ZnO NPs (the average particle size) and 100 μg mL^{-1} of 87 nm ZnO NPs (the average particle size) after 24 h of exposure (Fig. 6a and c). As compared to the control group, 7.1-fold and 33-fold increase of late apoptotic and necrotic cells were induced by 100 μg mL^{-1} of 24 nm ZnO NPs (the average particle size) in 2D cell model, respectively, but 4.2-fold, 12.5-fold, and 3.5-fold increase of early apoptotic, late apoptotic, and necrotic cells in 3D cell culture, respectively (Fig. 6a and b). Cultures exposed to 100 μg mL^{-1} ZnO NPs showed a severe decrease (12.9%, and 24.6% for 24 nm and 87 nm ZnO NPs (the average particle size)) in the number of viable 2D cells when compared with the control (about 95%), whilst slight decrease (73.9%, and 75.3% for 24 nm and 87 nm ZnO NPs (the average particle size)) of viable cells in 3D model. After 24 h of high-concentration ZnO NPs treatment (75 μg mL^{-1} and 100 μg mL^{-1}) in the 2D model, the main mode of cell death is necrosis rather than apoptosis, but there are opposite result was observed at lower concentrations of ZnO NPs (below 50 μg mL^{-1}) (Fig. 6a and c). In addition, the main mode of cell death observed in the 3D model is also predominantly apoptotic at various concentrations of ZnO NPs (above 10 μg mL^{-1}) (Fig. 6b and d).

4. Discussion

Caco-2 cell as an *in vitro* model of the human small intestine mucosa is widely used across the pharmaceutical industry to predict the absorption of orally administered drugs. The cells are approximately 40 to 70 μm and spindle-shaped or polygon-shaped (high cell density) with adherent cells growing as a confluent monolayer. This study used human colon cell line, since ZnO NMs have been incorporated into some consumer products such as dietary supplements, food additives and food

ZnO NPs (the average particle size) at (i) 12 h, or (j) 24 h, and 87 nm ZnO NPs (the average particle size) at (k) 12 h, or (l) 24 h. Values are mean ± SE from minimum three independent experiments. *p* < 0.05, α significantly different from control group (ctrl).
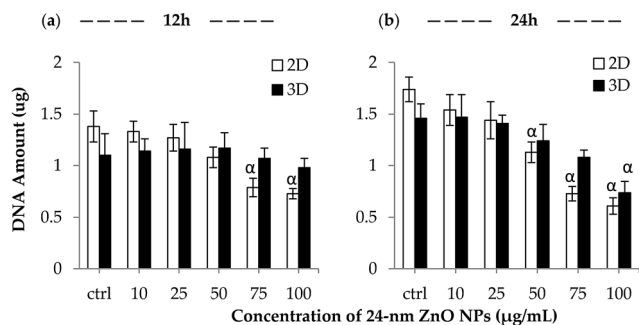
Fig. 5 Changes in DNA levels of 2D and 3D cells with various ZnO NP concentrations by DNA assay at (a) 12 h and (b) 24 h. Data represent mean ± SE, $n = 3$. $p < 0.05$, α significantly different from control group (ctrl).
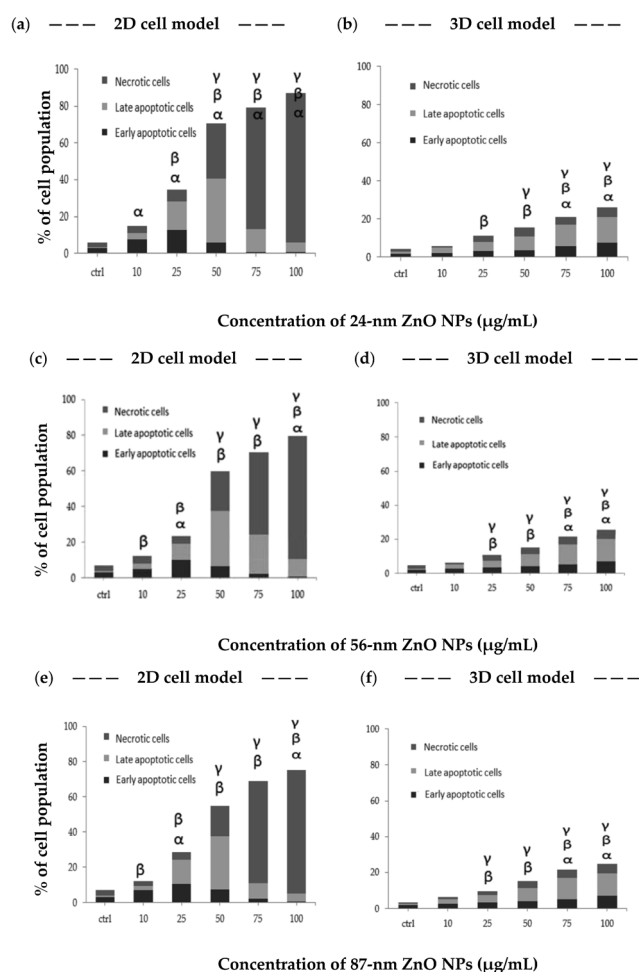

Fig. 6 Quantitative apoptotic measurement of 2D and 3D cells induced by ZnO NPs for 24 h. Different modes of cell death were induced by 24 nm ZnO NPs (the average particle size) in (a) 2D cell model and (b) 3D cell model, 56 nm ZnO NPs (the average particle size) in (c) 2D cell model, (d) 3D cell model. $p < 0.05$, 87 nm ZnO NPs (the average particle size) in (e) 2D cell model, (f) 3D cell model. $p < 0.05$, α significantly different with the percentage of early apoptotic cells in control group (ctrl), β significantly different with the percentage of late apoptotic cells in ctrl, γ significantly different with the percentage of necrotic cells in ctrl.

packaging.[35] The primary objective of this work was aimed at assessing the impact of different-sized ZnO NPs on Caco-2 cell toxicity and inflammatory response among different concentrations in 2D and 3D culture environment, in turn re-evaluate their perceived high toxicity of ZnO NPs based on 2D cell model.

Previous studies reported that *in vivo* cancerous cells could utilize ROS as a signaling molecule to promote their cell proliferation and metastasis.[36,37] Our observation was consistent with this notion, similarly showed that the 3D cells displayed higher levels of basal ROS as compared to the 2D cells. Fig. 3 indicated that the cells in 3D culture could replicate this *in vivo* characteristic, while the high ROS characteristics dissipated when the cells were cultured in 2D format. The percentages of 2D cells with cytoplasmic ROS levels increase in a time-dependent and dose-dependent manner to ZnO NPs exposure, but no significant elevation of ROS was observed in 3D cell model in the time and concentration studied. Similar 2D findings were reported by Kang *et al.*, who suggested that ZnO NPs induced oxidative stress in a dose-dependent manner.[30] ZnO NP-induced differential expression of intracellular ROS levels in 2D and 3D cell model indicated that the cellular responses to ZnO NPs were dependent on the cell culture systems. On the other hand, further studies involving downstream events of oxidative stress are needed to explore the underlying toxicity mechanism of ZnO NPs in 2D and 3D cell model. Downstream events of ROS include inflammatory response,[38,39] membrane damage,[40] DNA damage,[41] and these downstream damages can induce cell death.[42,43]

The production of IL-8 and IL-1β induced significant effects on the transcriptional and post-translational levels as they broadly affect inflammatory response.[44] After 12 h of high-concentrations ZnO NPs (above 50 μg mL^{-1}) exposure, the levels of IL-8 and IL-1β protein were significantly increased in 2D and 3D cell model except 2D cells for IL-8 (Fig. 4). The levels of IL-8 and IL-1β were further increased in 2D cell model, whilst decrease of the two proteins was observed in 3D cell model and the levels of IL-8 were even lower than the basal level of the control groups by 24 nm ZnO NP at 100 μg mL^{-1} for 24 h. These results indicated that ZnO NPs induced a chronic inflammatory response in 2D cell culture but acute inflammatory response in 3D cell culture. 24 nm ZnO NPs exposure increased highest levels of the two proteins in 2D cell model, but less levels of IL-8 than 87 nm ZnO NPs in 3D culture at 24 h. Expression of pro-inflammatory cytokines is not highly influenced by particle size in 3D cell model. Therefore, cellular microenvironment can dramatically affect the cellular responses to NMs. ZnO NPs induced inflammatory responses which is independent of ROS levels. ZnO NPs in 2D and 3D cell culture could induce undesirable intracellular ROS, inflammatory responses in preceding sections. At the same time, we further explored whether ZnO NPs also induce different effects on cell proliferation in 2D and 3D cell culture.

In Fig. 5, the DNA amounts of 2D cells were decreased at various concentrations of ZnO NPs in a dose-dependent manner. Interestingly, there were no significant differences in the DNA amounts of 2D cells among various concentrations of ZnO NPs at 12 h, but the amount of DNA was significantly

decreased since 100 µg mL^{-1} of ZnO NPs in 3D cell model, and since 50 µg mL^{-1} of ZnO NPs in 2D cell model (Fig. 5b). This result showed that Caco-2 cells in 3D culture could tolerate a higher concentration of ZnO NPs than the cells in 2D culture. In addition, the 2D cells displayed higher levels of cell proliferation as compared to the 3D counterpart between the control groups at 12 and 24 h, indicating that the 2D cells divided more actively than the 3D cells. However, it raises a concern about long term exposure to ZnO NPs can lead to accumulation of cell damage, as severe decrease of the DNA amounts were detected in 3D model after 24 h of exposure. To get more clues about the toxicity mechanism of ZnO NPs, we next profiled and quantified the mode of cell death (apoptosis and necrosis) for 2D and 3D cells exposure to ZnO NPs.

Fig. 6 showed 3D cells have a reduced response to the toxicity of ZnO NMs as compare to 2D cells, but two types of cells responded to ZnO NP toxicity in a dose-dependent manner after 24 h of exposure. ZnO NPs exposure has a particle size effect on 2D cells, but no difference in 3D model. The main mode of cell death was necrosis rather than apoptosis in the 2D model, whilst was predominantly apoptotic in the 3D model. Because ZnO NMs are a relatively harder material than the cell membrane, can eventually lead to cell necrotic death as the accumulation of the NMs impacted and damaged the membrane integrity.[45] A higher exposed area to the accumulated NPs lead to more necrosis as the 2D cell has more spread-out and squamous-type morphology than Caco-2 cell in 3D culture.

In the present study, ZnO NP-induced differential the results of previously described assays indicated that the significant effects of cell-culture models to cellular responses. Actively proliferating cells were previously reported to be more susceptible to certain drugs than quiescent cells.[46] The same might occur for interactions between cells and ZnO NPs. The 2D cells were more actively dividing as previously described results in Fig. 5, so they tend to take in more nutrients from their surroundings and in turn absorb more ZnO NPs. All in all, the toxic effects of ZnO NPs might be overestimated from the nanotoxicity results of 2D cell, at least in this study. May is the interaction between cells and cell matrix, have led to this result. Consistent with this result, previous studies similarly showed that the 2D cell culture overestimate the toxicity of test substances.[47,48]

5.   Conclusions

In summary, the toxicity of ZnO NPs on Caco-2 cells in 3D model was as follows; accumulated ZnO NPs in the cells elevated intracellular ROS expression inconspicuously, induced acute inflammatory response, significantly decreased the DNA amounts only at high concentrations and induced the toxicity independent of particle size. These events could eventually lead to cell apoptosis rather than cell necrosis. Interestingly, an opposite toxic mechanism of ZnO NPs was observed in our 2D cell model. This study suggested that understanding on how ZnO NPs induced different effects on Caco-2 cells under the simulated *in vivo* circumstance is very important, and acted as a precursor to other interesting experiments involving other NMs and 3D models. Caco-2 cells as intestinal epithelial cells would secrete mucin. The mucin secretion between 2D and 3D culture may be different, which could, in turn, causes different toxicity profiles. In the future, it is also necessary to study regarding mechanisms of cytotoxicity due to ZnO NPs in accordance with the cell types.

Author contributions

Zhipan Wu, Miao Tao, Rongfa Guan, Fei Lyu, and Mingqi Liu conceived and designed the experiments; Zhipan Wu and Miao Tao performed the experiments; Rongfa Guan, Fei Lyu, Guozhou Cao, and Jianguo Gao analyzed the data; Rongfa Guan wrote the paper.

Conflicts of Interest

The authors declare no competing financial interest.

Abbreviations

ZnO NPs	Zinc oxide nanoparticles
ROS	Reactive oxygen species
PI	Propidium iodide
VA	Early apoptotic cell
NVA	Late apoptotic cell
NVN	Necrotic cell

Acknowledgements

References

1 A. E. Nel, L. Mädler, D. Velegol, T. Xia, E. M. Hoek, P. Somasundaran, F. Klaessig, V. Castranova and M. Thompson, *Nat. Mater.*, 2009, **8**, 543–557.

2 A. Nel, T. Xia, L. Mädler and N. Li, *Science*, 2006, **311**, 622–627.

3 M. A. Dobrovolskaia and S. E. McNeil, *Nat. Nanotechnol.*, 2007, **2**, 469–478.

4 G. Veronesi, A. Deniaud, T. Gallon, P. H. Jouneau, J. Villanova, P. Delangle, M. Carriere, I. Kieffer, P. Charbonnier, E. Mintz and I. Michaud-Soret, *Nanoscale*, 2016, **8**, 17012–17021.

5 C. Y. Tay, M. I. Setyawati, J. Xie, W. J. Parak and D. T. Leong, *Adv. Funct. Mater.*, 2014, **24**, 5936–5955.

6 S. L. Chia and D. T. Leong, *Heliyon*, 2016, **2**, e00177.

7 Y. Gong, Y. Ji, F. Liu, J. Li and Y. Cao, *J. Appl. Toxicol.*, 2016, DOI: 10.1002/jat.3415.

8 G. D. Venkatasubbu, R. Baskar, T. Anusuya, C. A. Seshan and R. Chelliah, *Colloids Surf., B*, 2016, **148**, 600–606.

9 M. Chevallet, B. Gallet, A. Fuchs, P. H. Jouneau, K. Um, E. Mintz and I. Michaud-Soret, *Nanoscale*, 2016, **8**, 18495–18506.

10 H. Page, P. Flood and E. G. Reynaud, *Cell Tissue Res.*, 2013, **352**, 123–131.

11 D. W. Hutmacher, *Nat. Mater.*, 2010, **9**, 90–93.

12 J. Lee, M. J. Cuddihy and N. A. Kotov, *Tissue Eng., Part B*, 2008, **14**, 61–86.

13 L. G. Griffith and M. A. Swartz, *Nat. Rev. Mol. Cell Biol.*, 2006, **7**, 211–224.

14 S. L. Chia, C. Y. Tay, M. I. Setyawati and D. T. Leong, *Small*, 2016, **12**, 647–657.

15 M. Lutolf and J. Hubbell, *Nat. Biotechnol.*, 2005, **23**, 47–55.

16 C. Y. Tay, M. S. Muthu, S. L. Chia, K. T. Nguyen, S. S. Feng and D. T. Leong, *Adv. Funct. Mater.*, 2016, **26**, 4046–4065.

17 B. Feigl and D. Hutmacher, *Adv. Healthcare Mater.*, 2013, **2**, 1056–1062.

18 M. J. Bissell, A. Rizki and I. S. Mian, *Curr. Opin. Cell Biol.*, 2003, **15**, 753.

19 S. L. Chia, C. Y. Tay, M. I. Setyawati and D. T. Leong, *Small*, 2015, **11**, 702–712.

20 C. M. Sayes, K. L. Reed and D. B. Warheit, *Toxicol. Sci.*, 2007, **97**, 163–180.

21 T. R. Pisanic, J. D. Blackwell, V. I. Shubayev, R. R. Fiñones and S. Jin, *Biomaterials*, 2007, **28**, 2572–2581.

22 A. Magrez, S. Kasas, V. Salicio, N. Pasquier, J. W. Seo, M. Celio, S. Catsicas, B. Schwaller and L. Forró, *Nano Lett.*, 2006, **6**, 1121–1125.

23 C. M. Sayes, J. D. Fortner, W. Guo, D. Lyon, A. M. Boyd, K. D. Ausman, Y. J. Tao, B. Sitharaman, L. J. Wilson and J. B. Hughes, *Nano Lett.*, 2004, **4**, 1881–1887.

24 Y. Zhang, W. Chen, J. Zhang, J. Liu, G. Chen and C. Pope, *J. Nanosci. Nanotechnol.*, 2007, **7**, 497–503.

25 C. M. Sayes, A. A. Marchione, K. L. Reed and D. B. Warheit, *Nano Lett.*, 2007, **7**, 2399–2406.

26 Z. Liu, C. Davis, W. Cai, L. He, X. Chen and H. Dai, *Proc. Natl. Acad. Sci. U. S. A.*, 2008, **105**, 1410–1415.

27 K. M. Yamada and E. Cukierman, *Cell*, 2007, **130**, 601–610.

28 F. Pampaloni, E. G. Reynaud and E. H. Stelzer, *Nat. Rev. Mol. Cell Biol.*, 2007, **8**, 839–845.

29 D. M. Bryant and K. E. Mostov, *Nat. Rev. Mol. Cell Biol.*, 2008, **9**, 887–901.

30 T. Kang, R. Guan, X. Chen, Y. Song, H. Jiang and J. Zhao, *Nanoscale Res. Lett.*, 2013, **8**, 1–8.

31 R. Mauck, X. Yuan and R. Tuan, *Osteoarthritis Cartilage*, 2006, **14**, 179–189.

32 M. H. Wu, J. P. Urban, Z. F. Cui, Z. Cui and X. Xu, *Biotechnol. Prog.*, 2007, **23**, 430–434.

33 C. Monteiller, L. Tran, W. MacNee, S. Faux, A. Jones, B. Miller and K. Donaldson, *Occup. Environ. Med.*, 2007, **64**, 609–615.

34 W. C. Cho and K. N. Leung, *Cancer Lett.*, 2007, **252**, 43–54.

35 D. Loessner, S. C. Rizzi, K. S. Stok, T. Fuehrmann, B. Hollier, V. Magdolen, D. W. Hutmacher and J. A. Clements, *Biomaterials*, 2013, **34**, 7389–7400.

36 S. L. Payne, B. Fogelgren, A. R. Hess, E. A. Seftor, E. L. Wiley, S. F. Fong, K. Csiszar, M. J. Hendrix and D. A. Kirschmann, *Cancer Res.*, 2005, **65**, 11429–11436.

37 J. P. Fruehauf and F. L. Meyskens, *Clin. Cancer Res.*, 2007, **13**, 789–794.

38 M. Giovanni, C. Y. Tay, M. I. Setyawati, J. Xie, C. N. Ong, R. Fan, J. Yue, L. Zhang and D. T. Leong, *Environ. Toxicol.*, 2015, **30**, 1459–1469.

39 X. Cheng, W. Zhang, Y. Ji, J. Meng, H. Guo, J. Liu, X. Wu and H. Xu, *RSC Adv.*, 2013, **3**, 2296–2305.

40 W. Lin, Y. Xu, C. C. Huang, Y. Ma, K. B. Shannon, D. R. Chen and Y. W. Huang, *J. Nanopart. Res.*, 2009, **11**, 25–39.

41 V. Sharma, D. Anderson and A. Dhawan, *J. Biomed. Nanotechnol.*, 2011, **7**, 98–99.

42 M. I. Setyawati, C. Y. Tay and D. T. Leong, *Biomaterials*, 2013, **34**, 10133–10142.

43 M. I. Setyawati, X. Yuan, J. Xie and D. T. Leong, *Biomaterials*, 2014, **35**, 6707–6715.

44 T. Strowig, J. Henao-Mejia, E. Elinav and R. Flavell, *Nature*, 2012, **481**, 278–286.

45 G. DeLoid, J. M. Cohen, T. Darrah, R. Derk, L. Rojanasakul, G. Pyrgiotakis, W. Wohlleben and P. Demokritou, *Nat. Commun.*, 2014, **5**, 3514.

46 R. Schulz, F. Streller, A. Scheel, J. Rüschoff, M. Reinert, M. Dobbelstein, N. Marchenko and U. Moll, *Cell Death Dis.*, 2014, **5**, e980.

47 U. G. Sauer, S. Vogel, A. Hess, S. N. Kolle, L. Ma-Hock, B. van Ravenzwaay and R. Landsiedel, *Toxicol. In Vitro*, 2013, **27**, 174–190.

48 W. S. Cho, R. Duffin, M. Bradley, I. L. Megson, W. MacNee, J. K. Lee, J. Jeong and K. Donaldson, *Part. Fibre Toxicol.*, 2013, **10**, 1.